Ecole Nationale Supérieure

de Chimie, Biologie et Physique

SYNTHESE DE STAGE DE SPECIALISATION

Département CGP

Towards the optical generation of 1THz bandwidth acoustic wavepackets for the detection of buried nanostructures

RICHARD DE LATOUR Hugo

Spécialisation : *Nano- et Micro- Technologies*

Nom de la Société : ARCNL

Secteur d'activité : Recherche

Stage effectué du 01/05/2020 au 30/09/2020

Maître de stage industriel : Prof. Dr. P. C. M. Planken

Tuteur ENSCBP : M. Toutain

Acknowledgements

Contents

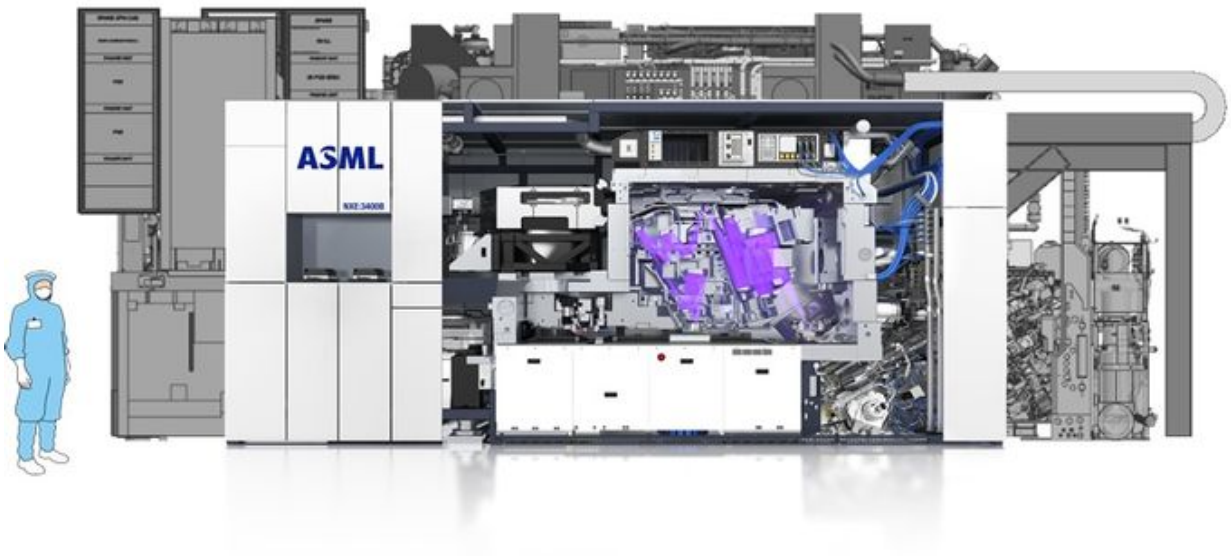

Figure 1: ASML Nanolithography Machine [1]. ASML's nanolithography equipment can cost several hundred million euros.

ARCNL

ADVANCED RESEARCH CENTER FOR NANOLITHOGRAPHY

Figure 2: ARCNL's logo.

I ARCNL

To complete my studies at the ENSCBP I was offered the opportunity to do a 22-week internship at ARCNL in the Light-Matter Interaction Group, alongside Prof. Dr. Paul Planken.

I. A ASML

ASML (Advanced Semiconductor Materials Lithography) is a Dutch company, which produces photolithography systems for the semiconductor industry. It was founded in 1984 in Eindhoven, The Netherlands by Philips and ASMI (Advanced Semiconductor Materials International), in order to develop new lithography solutions for the growing semiconductor industry [2]. In their 36 years of existence, they have become a figurehead and the leading supplier of the semiconductor industry, as most of the biggest semiconductor fabrication plants worldwide have integrated ASML's machines. ASML has managed to attain this position by enabling the fabrication of smaller and smaller features, using increasingly higher frequency light sources. Figure 1 shows one of ASML's latest Extreme-UltraViolet (EUV) lithographic equipment. This new generation of lithography machines uses EUV light (13.5 nm) instead of Deep-UltraViolet (DUV) light sources (193 nm), paving the way to resolutions under 45 nm.
It is its research that has established ASML, and it is still proud to be a research-driven company, with over two billion euros (17% of their annual revenue) spent in research expenses each year [3]. Over the years, ASML has had to tackle many scientific challenges in order to become who they are today. As the time passes, these challenges become more and more complex and requires very-early research in order to stay competitive. To do so, ASML partners with academia and research centers.

I. B ARCNL

The Advanced Research Center for NanoLithography (ARCNL) (logo on figure 2) is a fairly recent research center based in Amsterdam, as it was created in 2014 [4]. It stemmed from a public/private collaboration of the University of Amsterdam, the Vrije Universiteit and ASML. Thus, ARCNL combines the universities' scientific quality output, their research freedom, and their teaching focus; and ASML's application-based interests.

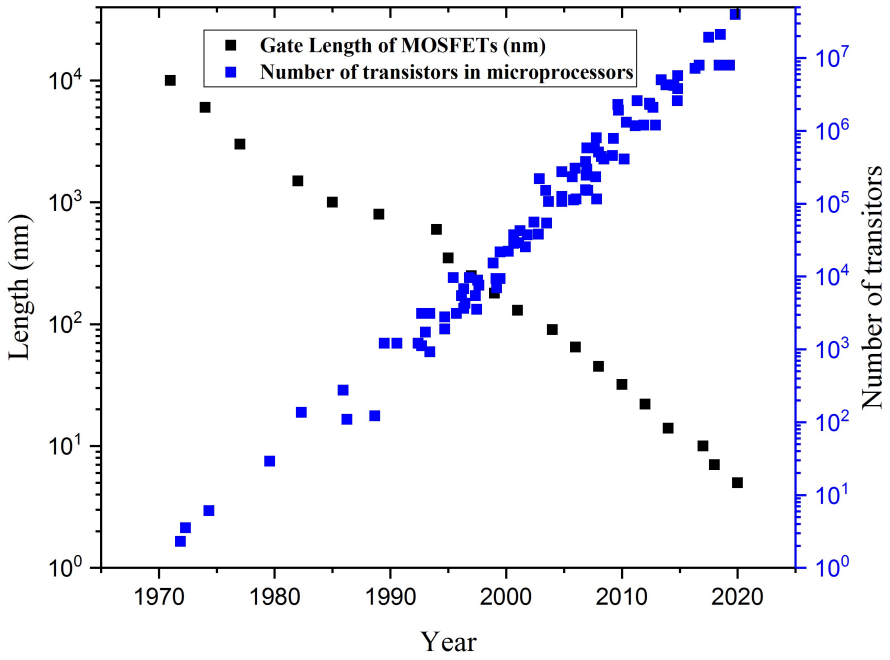

Figure 3: Gate length of MOSFETs and number of transistors in microprocessors as a function of time [5, 6]. This graph represents Moore's Law. Since the 70s, the semiconductor industry has been able to downsize their processes to create ever-so-tiny components, while integrating skyrocketting amounts of components on chips, therefor, increasing their complexities.

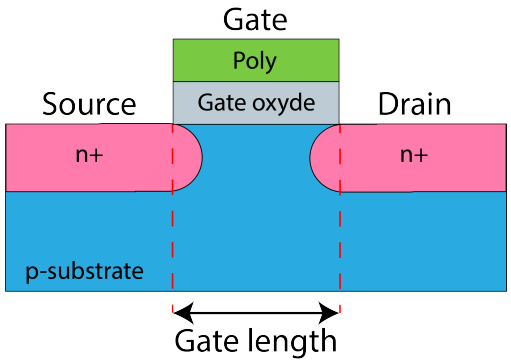

Figure 4: Schematic of an n-channel MOSFET. The gate length is typically the characteristic that the semiconductor industry uses to define the size of a transistor.

I. C Light-Matter Interaction Group

In ARCNL, I joined the Light-Matter interaction group. One of its mission is to study how short light pulses can generate high frequency ultrasounds in many materials. The purpose of this research is that while many materials are opaque to light, few are opaque to sound. Thus, the idea is to use sound waves travelling in materials to probe interfaces hidden underneath opaque layers. It is comprised of its team leader, Prof. Paul Planken, a technician, one postdoc and three PhD students.

II Introduction

In this report, I will present the work I produced at ARCNL towards the optical generation of 1THz bandwidth acoustic wavepackets for the detection of buried nanostructures. In order to understand the appeal of such a subject, we first need to discuss its context.

II. A Context of the project

As explained earlier in this report, most of the research projects at ARCNL stem from real-world problems at ASML. Since the 70s, the targets set by the semiconductor industry have been motivated by Moore's Law. Moore's Law is an observation-based projection, forecasting the never-ending increase of complexity of silicon chips [7]. The semiconductor industry has tackled the issue by shrinking electronic components in order to increase the number of components per chip as shown in figure 3. In the 60s, the first metal-oxide-semiconductor field-effect transistors MOSFET, see figure 4) had 10 μm gate lengths; today Samsung and TSMC are building fabrication plants which will produce 3 nm gate length MOSFETs [8, 9].

Building these ever-so-tiny electronic components often requires precisely piling several layers of different materials on top of each other. To make sure these different layers are properly aligned is critical and has become a challenge by itself. To do so, so-called "alignment gratings" are etched on the wafers, as shown on figure 5. They are used as diffraction gratings. When light illuminates the grating, some of it will be diffracted by the grating. Slight translation of the wafer will change the phase-difference of the $+n^{th}$ and the $-n^{th}$ diffracted orders, which is detectable via interference. This method is extremely precise and can detect nanometer-scale misalignment [10]. However, this tech-

Figure 5: Example of an alignment target consisting of four gratings. The top-left and bottom-right quadrants are two X-gratings with a slightly different pitch of 16 μm and 17.6 μm , respectively. The top-right and bottom-left gratings are Y-gratings with the same slightly different pitches [10]

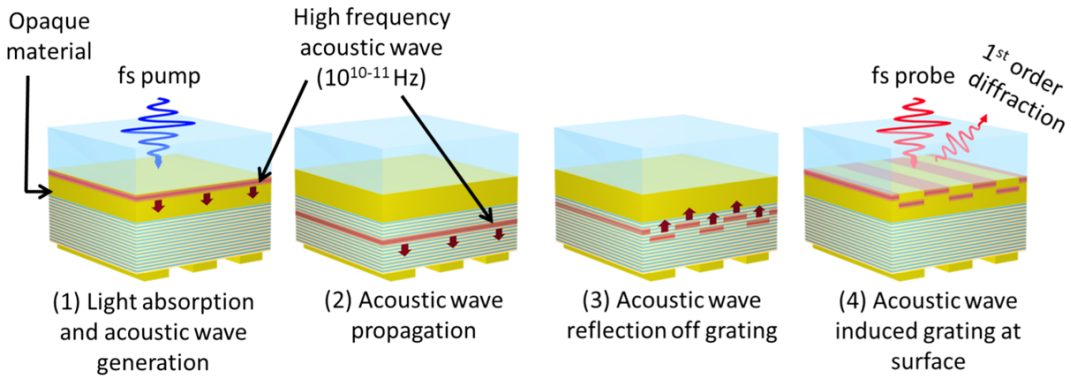

Figure 6: Schematic explaining the concept. A laser pulse is absorbed by the material at the substrate-material interface (1), launches an acoustic wave that propagates through different layers (2). The acoustic wave reflects off the buried grating and returns to the substrate-material interface as a grating-shaped acoustic wave (3). The time-delayed probe pulse diffracts off this interface grating, and the first-order diffraction signal is recorded (4). This picture was taken from Dr. Stephen Edward's PhD Thesis [11]

nique requires for the materials on top of the grating to be optically transparent. This limits greatly the complexity of possible device architecture.

The Light-Matter Interaction group is looking into a possible way to circumvent such issues. The key reasoning behind their solution is that whilst some materials are opaque to light, only few are opaque to sound. Thus, it is possible to ”see” a buried interface by launching acoustic waves in a material, and analysing the echoes. Figure 6 gives a great illustration of this method.

As mentioned above, we will dive into the optical generation of 1 THz bandwidth acoustic wavepackets for the detection of buried nanostructures. The idea behind this project is that we want to be able to probe interfaces (such as alignment gratings) underneath an optically opaque layer. The ultimate resolution of this method will be dependant upon the spectral broadness of the acoustic wavepacket. Here, the goal is to increase the central frequency of the acoustic wavepackets to the THz-region. Typically, in the field of high-frequency laser ultrasonics, the acoustic wavepackets have central frequencies of a few hundred GHz [12]. By launching THz acoustic pulses, we hope to increase the resolution of this technique.

II. B Scientific Background

In order to understand the rest of the work reported here, it is important to understand some key concepts first.

II. B. 1 High-Frequency Laser Ultrasonics

Laser Ultrasonics refers to the field that studies the generation and the detection of acoustic waves by lasers. It is extensively used in material testing in different industries (aeronautics, composites, microelectronics, metallurgy, polymers, etc...) [13]. For most laser ultrasonics applications, a few MHz acoustic waves are used. For the detection of nanometer-scale structures however, higher frequencies are necessary. To achieve this, the surface is illuminated with lasers with short pulse lengths (we use a femtosecond laser). In our experiments, we use so-called pump-probe experiments, in which a highly energetic pump pulse modifies the sample, and a time-delayed, less energetic probe pulse detects the transient changes induced by the pump pulse.

$$C_e(T_e)\frac{\partial T_e}{\partial t} = \nabla(\kappa_e \nabla T_e) - \Gamma(T_e - T_l) + Q(\vec{r},t) \tag{1}$$

$$C_l\frac{\partial T_l}{\partial t} = \nabla(\kappa_l \nabla T_l) + \Gamma(T_e - T_l) \tag{2}$$

Equation 1 : The Two-Temperature Model. This model is defined by two equations, (1) describes the evolution of the electron temperature and (2) describes that of the lattice. It includes thermal diffusion terms "$\nabla(\kappa\nabla T)$" for both the electrons and the lattice, an exchange term between the lattice and the electrons "$\Gamma(T_e - T_l)$", and an extra term for the electron gas representing the original source of heat"$Q(\vec{r},t)$". C_e and C_l are the heat capacities of the electron gas and the lattice. Note that for the electron gas, the heat capacity is temperature-dependant which comes from the Fermi distribution of electrons. κ_e and κ_l are the thermal conductivities of the electron gas and the lattice. Γ is the electron-phonon coupling constant, it translates how easy it is for the electron gas to exchange heat with the lattice.

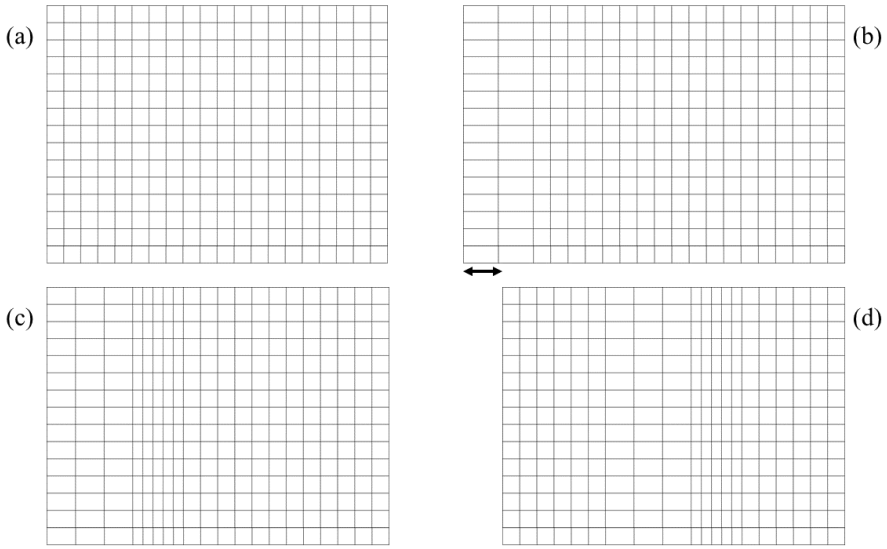

Figure 7: Schematic of the launch of an acoustic wave. (a) represents a crystal lattice as a 2D lattice of bobs attached together by springs, at rest. (b) the increase in lattice temperature forces the irradiated surface of the cube to expand outwards, causing surface displacement. (c) just like with a rubber band, this causes the launch of a longitudinal acoustic wave. (d) the acoustic wave will travel from the surface onto which we applied the force to the opposite side.

Generation of high-frequency ultrasounds in solids. The response of a given material to a light pulse irradiating its surface is dependent on the material's electronic structure. The complex dielectric function of a material $\tilde{\epsilon}$ is a useful tool to understand this response. It is given by $\tilde{\epsilon} = \epsilon_0(n_1^2 - n_2^2 + in_1^2n_2^2)$, where ϵ_0 is the vacuum dielectric constant, n_1 is the refractive index, and n_2 is the extinction coefficient. The extinction coefficient is related to the penetration depth of the light in a material by the relation $d_p = \frac{c}{n_2\omega}$, where c is the speed of light and ω is the angular frequency. The penetration depth is the depth at which the intensity of the a light pulse has diminished by $\frac{1}{e}$ of the value at the surface. In metals with non-zero extinction coefficients a part of the light will be absorbed as heat by the material's free electrons.

Free electrons in a metal can be treated like a monoatomic gas to the exception that electrons obey Fermi-Dirac statistics (meaning by this that electrons are fermions which obey the Pauli exclusion principle stating that two particles cannot occupy the same quantum state). We can thus define an electron temperature T_e separate from the lattice temperature T_l. When the electron gas absorbs light, the temperature of the electrons mostly within the penetration depth increases in a matter of a few hundred femtoseconds, referred to as the electron gas thermalization time. If the metal is thicker than the penetration depth, this creates a gradient between the heated surface electrons and the cool bulk electrons. The Two-Temperature Model (TTM) (see equation 1), introduced by *Anisimov et al.* [14], describes the behaviour over time of both the electron temperature and the lattice temperature. In this model, an exchange term is responsible for transferring heat from the electrons to the lattice and is null when both temperatures are equal. As the temperature of the lattice increases, this will induce an isotropic thermal stress, responsible for the thermal expansion of the lattice.

Note that in the case where the sample is much thicker than its penetration depth, the thermal expansion of the lattice only happens from the surface down to a few nanometers (depending on the optical penetration depth of the material and the electron and lattice thermal conductivities). As shown in figure 7, the surface thermal expansion of the lattice generates a normal acoustic wave travelling from the illuminated surface. It is worth noting that the reason the thermal strain is not diluted into the bulk of the material is because of the timescales we are dealing with here. The acoustic wave is generated in the first picoseconds after illumination. The acoustic wave can be described classically as a linear elastic longitudinal wave.

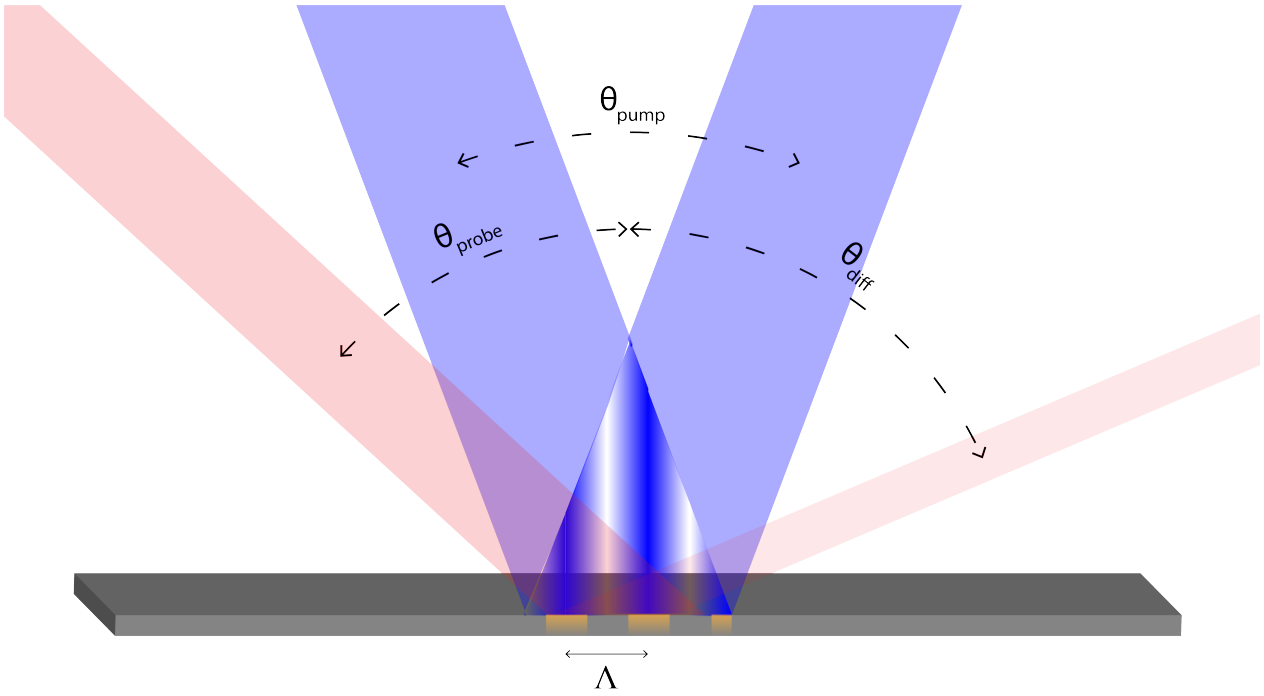

Figure 8: Schematic of the transient grating geometry. The sample is illuminated with two pump beams (blue) with an angle θ_{pump} in a way that they interfere at the surface of the sample with a periodicity Λ. This produces a grating (orange) which a probe beam (red) at an angle θ_{probe} will get diffracted upon at an angle θ_{diff}.

Detection of high-frequency ultrasounds in solids. As mentioned above, the acoustic waves are detected optically. We are able to do so because the optical constants of the sample will be changed by the acoustic wave and the change in temperature. The complex dielectric function can be expressed as follows, $\tilde{\epsilon} = \tilde{\epsilon}^b + \tilde{\epsilon}^f$, where $\tilde{\epsilon}^b$ is the contribution of bound electrons to the complex dielectric function, and $\tilde{\epsilon}^f$ is that of free electrons.

The complex dielectric function of free electrons depends on the plasma frequency ω_p, itself dependant on the electron density n_e, which an acoustic wave will change.

Additionally, the rise in the electron temperature will change the Fermi distribution in the material (more states in the conduction band become populated by electrons previously in the valence band). Thus, increasing the probability for intraband transitions, related to the complex dielectric function of bound electrons.

In brief, there are two mechanisms responsible for the change of the optical properties in our experiments :

• the change of the electron temperature

• the change of the material's density

II. B. 2 Transient Grating

In our experiments, we use a so-called transient grating geometry to generate the acoustic waves in our sample. As shown in figure 8, this means that we make two pump beams interfere on the surface of our sample, so as to illuminate it with an interference pattern.

The three beams (two interfering pump beams and a probe beam) must be spatially and temporally overlapping on the surface of the sample. If the pump beams are not overlapping, the transient grating is not created, and the probe has nothing to diffract from. If the pump beams are overlapping but the probe is not, the transient grating is created but is not probed. This overlap condition requires very precise alignment and construction. In practice, this is achieved by using a single light source divided in three beams with same path length.

The interference periodicity of the two pump beams Λ is given by $\Lambda = \frac{\lambda_{pump}}{sin(\theta_{pump}/2)}$, where λ_{pump} is the wavelength of the pump beams, and θ_{pump} is the angle between the two beams. Typically, we aim for this periodicity to be of a few micrometers (much larger than the sample thickness, which is

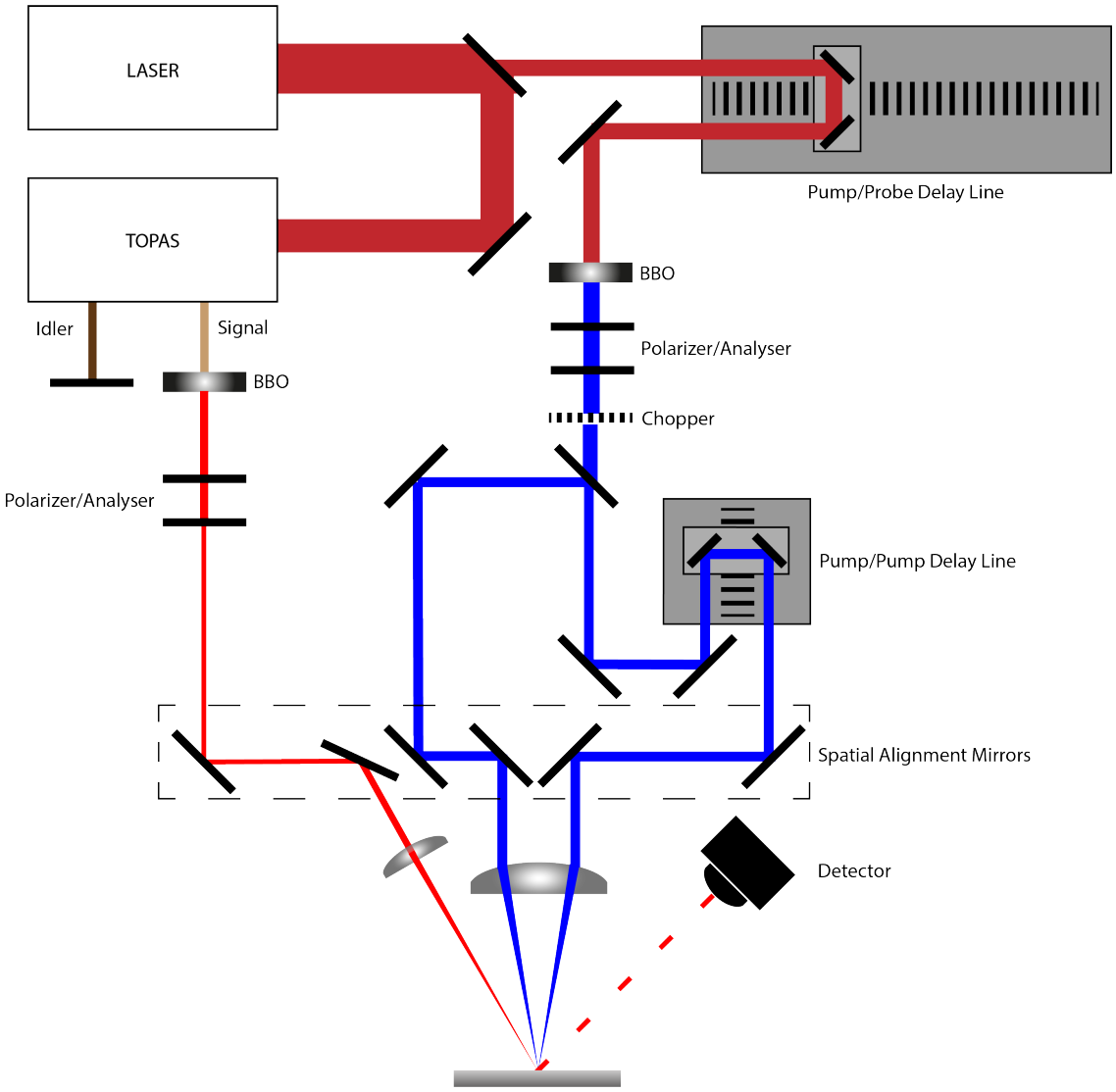

Figure 9: Schematic of the setup. The laser outputs a 800 nm beam (dark red) which is separated into two beams.
•a probe which goes into the TOPAS, which converts it to a 1300 nm beam (beige), which is then frequency doubled by a BBO crystal into a 650 nm beam (light red). It is then attenuated by a polarizer/analyser system, gets spatially aligned by two mirrors and gets focused onto the sample with a lens.
•a pump which travels through the pump/probe delay line, then gets frequency doubled by a BBO crystal into a 400 nm beam (blue). It is then attenuated by a polarizer/analyser system, it gets its repetition rate halved by the chopper, it gets divided by a beam splitter and one of the two pump beams travels through the pump/pump delay line. Each pump beam gets aligned so as to arrive parallel on a lens which will focus them on the sample.
Finally, an InGaAs detector receives the signal of the diffracted probe beam.

usually in the range of nanometers) so as to prevent thermal diffusion between the light and dark fringes. The surfaces illuminated by the light fringes will go through the processes described in the previous section, while the surface illuminated by the dark fringes will not be changed. This means that the optical parameters of the material under different fringes will be different. In other words, transient grating induces spatially periodic changes in the optical constants of the sample, which the probe beam can get diffracted from. Additionally, the spatially periodic surface displacement of the sample will also induce diffraction.

The diffraction efficiency η is defined as $\eta = \frac{P}{P_{probe}}$, where P is the power of the diffracted beam and P_{probe} is the probe power. In the scenario where the probe beam is incident at an angle θ_{probe}, the diffraction angle is $sin(\theta_{diff}) = sin(\theta_{probe}) - \frac{n\lambda_{probe}}{\Lambda}$, where n is an integer related to the diffraction order and λ_{probe} is the wavelength of the probe. Because the diffraction efficiency scales down as the diffraction order increases, we usually measure the first order diffraction.

The reason we use the transient grating geometry over measuring changes in reflection is that the transient grating geometry is background free as the diffraction efficiency is null when the pump does not hit the sample, whereas in reflection geometry, the background is never null.

III Experimental Details

In this section, we will describe the design of the optical setup we measured with and we will explain our experimental plan, so as to get a thorough understanding of the results.

III. A Setup

A schematic of the experimental setup is shown in figure 9. This setup is comprised of three main parts : a femtosecond laser, an optical parametric amplifier, and a transient grating geometry design.

The femtosecond laser used in this setup is an amplified Ti:Sapphire laser (Astrella, from Coherent) which outputs laser beams with a repetition rate of 1 kHz, a central wavelength of 800 nm, a pulse length of 35 fs and a pulse energy of 6 mJ. The laser pulses are divided in two beams with a 5/6 beam splitter. The least intense beam will become the pump beams, while the other will become the probe beam.

The probe beam is guided into an optical parametric amplifier (TOPAS) (HE-TOPAS, from Light Conversion). The role of the TOPAS is to generate higher wavelengths via optical parametric amplification. It outputs two laser beams (the idler and the signal) which frequencies add up to that of the incident beam. It can be set to output wavelengths from 1160 nm to 2400 nm. In our experiments, we set it to a central wavelength of 1300 nm and a pulse energy of 1 mJ.

The role of the 50% mechanical chopper on the pump path is to reduce its repetition rate to 500 Hz, as every other pump pulse is blocked by the chopper. This is useful to subtract background from the signal. The background is the diffraction efficiency when only the probe illuminates the sample. For every pump pulse hitting the sample, the probe will hit the sample twice; a background measurement and a diffraction measurement. The angle at which the pump beams arrive on the sample is calculated to give a periodicity of 6μm. Similarly, the probe beam is aligned so as to arrive at an angle of 30°on the sample.

As explained previously, the transient grating geometry relies on the spatial and temporal alignment of the three beams. Optimal spatial alignment is obtained using the spatial alignment mirrors, before the lenses. Temporal alignment is secured if all beam path lengths are equal. Because the processes we wish to measure happen in the realm of femtoseconds, the path length must have a micrometer-precision. This is ultimately achieved by the delay lines. The pump/pump delay line enables to have control over the temporal overlap of the two pump beams. The pump/probe delay line enables to have control over the temporal overlap of the pump beams with respect to the probe. The pump/probe delay line is computer-controlled, which makes it possible to measure the diffraction efficiency of the sample at different moments in regards to when the pump beams illuminate the surface.

III. B Experimental Plan

As discussed earlier in this report, the aim of this project is to study the possibility to generate THz acoustic waves in solids, in order to possibly increase the resolution of photoacoustic-based alignment techniques. We believe that one of the ways to achieve such a result is via choosing a material with the proper characteristics. The specifications for such a material are as follows :

• **High Extinction Coefficient** : The extinction coefficient is inversely proportional to the penetration depth. A short penetration depth will induce a very local deposition of the energy, which

Property	Au	Ru	Unit
Extinction Coefficient at 400 nm (n_2)	$1.9^{(a)}$	$4.8^{(b)}$	/
Electron-Phonon Coupling Constant$^{(c)}$ (Γ)	2.3	185	$10^{16} * W.m^{-3}.K^{-1}$
Electron Thermal Conductivity at 300K$^{(c)}$ (κ_e)	317	117	W .m^{-1}.K^{-1}

Table 1: Table comparing different properties of gold and ruthenium. (a) extracted from multiple sources from refractiveindex.info [15]. (b) measured by Dr. Stephen Edward via ellipsometry. (c) extracted from *Bonn et al.* [16].

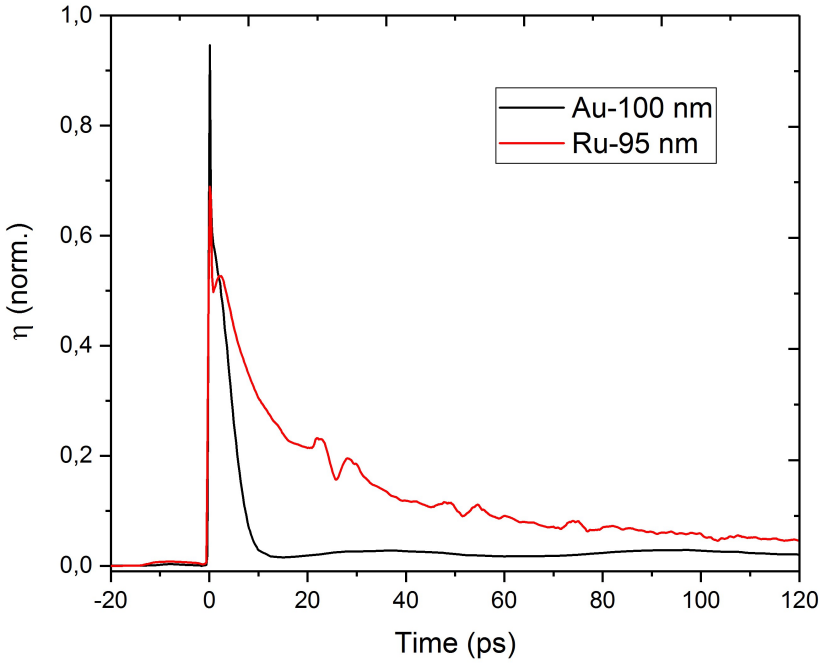

Figure 10: Normalized diffraction efficiency of a 100 nm-thick gold sample (black) and 95 nm-thick ruthenium sample (red), both on glass, as a function of time. t=0 is the moment when the two pump pulses create a transient grating on the surface of the sample. The signals were smoothed using a 2-points adjacent-average method.

is necessary given we aim to reduce the wavelength of the acoustic wave.

• **High Electron-Phonon Coupling and Low Electron Thermal Conductivity** : As shown in equation 1, the Two-Temperature Model takes two main processes into account : an electron thermal diffusion term, and an electron-phonon coupling term (the lattice thermal diffusion term is typically much weaker and is usually disregarded [16]). If the electron thermal diffusion term is greater than the electron-phonon coupling term, the electron gas will thermalize to a single temperature, before exchanging heat with the lattice. If the electron thermal diffusion term is weaker than the electron-phonon coupling term, than the hot electrons will exchange heat with the lattice before the temperature diffuses to the bulk electrons.

These parameters aim to restrain the distance from the surface over which the lattice initially expands after being illuminated (i.e. the central wavelength of the acoustic wave).

For the sake of this report, we will compare the photoacoustic responses of two materials, one which fits the specifications described above (ruthenium), and one which does not (gold), see figure 1. Second, we will also test both thick and thin samples of ruthenium, in order to further restrain the depth over which the acoustic wave is generated.

IV Results and Discussion

In this section we will present the results from our transient grating photoacoustic experiments on thin and thick films of gold and ruthenium. Dr. Stephen Edward prepared the samples (more details on the fabrication of the films is given in appendix A) and measured their thicknesses with an AFM.

IV. A Thick Films of Ruthenium and Gold

The thick films of ruthenium and gold we measured on were respectively 95 nm- and 100 nm-thick. The results from the transient grating experiments on these samples is shown on figure 10. These measurements were taken with a probe power of 1 mW and a pump power of 10 mW.

At t=0s, we observe a sudden increase in the diffraction efficiency of both samples. This can be explained by the rapid absorption of the light pulses by the electrons within the metal. The probe pulse is diffracting off the periodic change in electron temperature induced by the transient grating

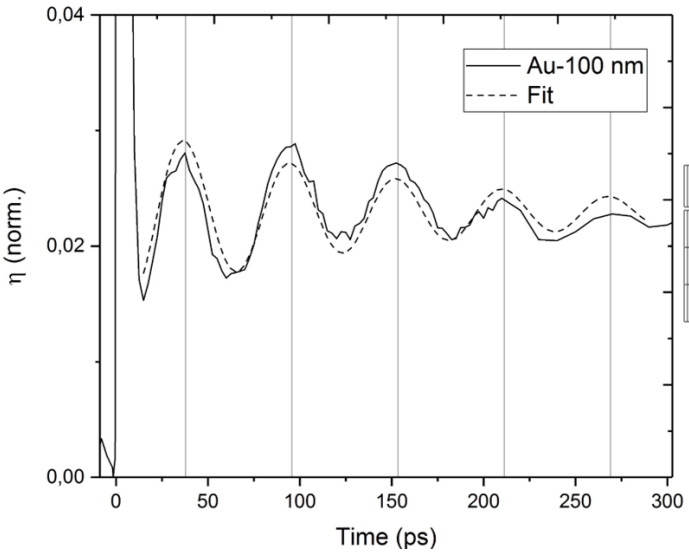

	Damped Sine
Equation	$\eta(t) = y_0 + A * exp(-t/t_0) * sin(2\pi\frac{t-\phi}{T})$
T	$57,8ps$
R^2	$0,82$

Figure 11: Sinusoidal behaviour of the diffraction efficiency in the 100 nm-thick gold sample (solid) and its fit (dotted). The signal was smoothed using a 2-points adjacent-average method. The table on the right gives the details of the fit.

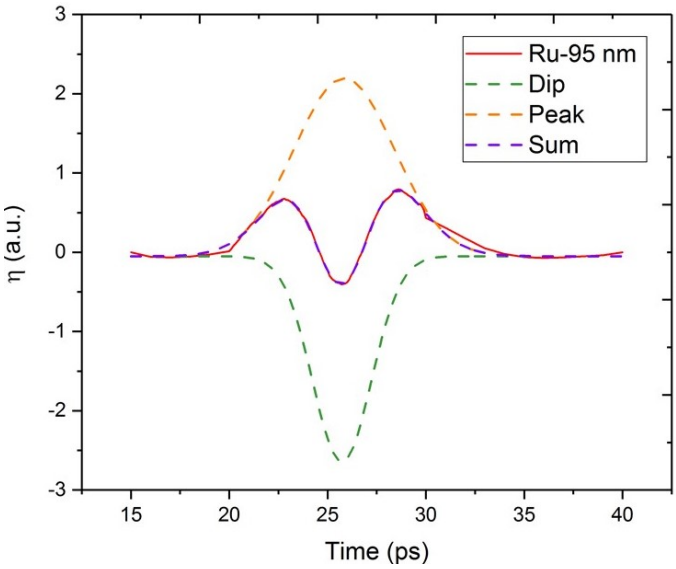

	Peak	Dip
Equation	$\eta(t) = \frac{2A\sqrt{ln(2)}}{FWHM\sqrt{\pi}} \times e^{-4(\frac{\sqrt{ln(2)}(t-t_c)}{FWHM})^2}$	
$FWHM$	5,98 ps	3,53 ps
Gaussian Position (t_c)	25,8 ps	25,7 ps

Figure 12: Periodically recurring pattern in the diffraction efficiency of a 100 nm-thick ruthenium sample. An exponential decay was subtracted from the signal, and it was smoothed using a 2-points adjacent-average method. This pattern was fitted by the sum of two gaussian functions (a dip and a peak). The table on the right gives the details of each of these gaussians such as the full-width at half-maximum (FWHM) and the gaussian position, which is the time around which the gaussian is centred.

geometry. This peak is referred to as the electron peak as it is controlled by electron dynamics after irradiation. At this point, the diffraction efficiency drops exponentially. This can be understood by the hot electrons exchanging heat with both the bulk, cold electrons and the lattice.
Then, the gold and the ruthenium samples display different behaviours. This should be attributed to their different properties, as shown on table 1.

100 nm-thick Gold layer From 10 ps on, the signal collected from the gold sample presents a sinusoidal shape that could be detected for over 300 ps. As shown on figure 11, the signal was fitted with a damped sine function, from which we found a periodicity of 57,8 ps. This periodicity coincides with the round trip time of an acoustic wave travelling through the layer. As a matter of fact $T = 57,8ps \approx \frac{2\times 100.10^{-9}m}{3240m/s} = \frac{2d}{v_{Au}}$, where T is the periodicity, d is the thickness of the film (100 nm) and v_{Au} is the longitudinal speed of sound in gold (3240 m/s) [17].
We mentioned above that gold had -compared to ruthenium- a higher electron thermal conductivity and a lower electron-phonon coupling. As a result, the hot electrons in gold will diffuse their energy to the cool, bulk electrons rapidly. We can assume that for a 100 nm-thick gold film, the temperature will be mostly distributed throughout the entire thickness. [18]. Eventually, the heat will be transferred to the lattice, and the entire thickness will experience thermal strain. This can be seen as a standing wave comprised of two counter-propagating acoustic waves with wavelength of twice the thickness of the layer. This explains our observation of a sinusoidal behaviour in the diffraction efficiency.

95 nm-thich Ruthenium layer In contrast to the measurements on gold, the ones on ruthenium do not exhibit a sinusoidal behaviour. They exhibit a second peak at 1,8 ps, followed by a periodically recurring pattern in the diffraction efficiency with a period of 25,7 ps, corresponding to the round trip time of an acoustic echo. This pattern is shown on figure 12. It is comprised of a dip, between two peaks. *Devos et al.* studied such patterns on tungsten, and concluded that this phenomena was due to the probe wavelength, and that this shape does not necessarily hold meaning on the actual acoustic wave [19].
With this in mind, we determined the temporal and spatial extent of the acoustic waves detected. The temporal width of an acoustic wave is defined as its full-width at half-maximum (FWHM), here

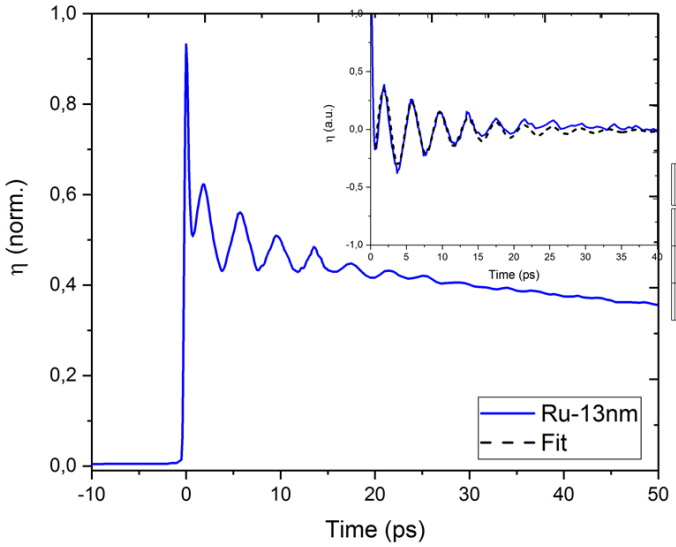

	Damped Sine
Equation	$\eta(t) = y_0 + A * e^{-t/t_0} * sin(2\pi\frac{t-\phi}{T})$
T	3,91 ps
R^2	0,94

Figure 13: Normalized diffraction efficiency of a 13 nm-thick ruthenium sample (blue), both on glass, as a function of time. The signal was smoothed using a 2-points adjacent-average method.

5,98 ps, or 167 GHz. The wavelength of the acoustic wave is $\lambda = v_{Ru} \times FWHM = \frac{2\times 95.10^{-9}m}{25,7.10^{-12}s} \times 5,98.10^{-12}s = 44,2nm$, where v_{Ru} is the longitudinal speed of sound in ruthenium, which we calculate with the round trip time and the film thickness.

This wavelength is much higher than the penetration depth of the pump in ruthenium (approximately 13 nm). This difference should be attributed to electron (and lattice) thermal diffusion. We can hypothesise that restraining the thickness of the film might generate higher-frequency acoustic waves.

IV. B Thin Film of Ruthenium

The thin film of ruthenium we measured on was 13 nm-thick. The results from the transient grating experiments on this samples is shown on figure 13. These measurements were taken with a probe power of 1 mW and a pump of 10 mW.

The signal we observed on this sample resembles the signal of the 100 nm-thick gold sample. Similarly, we can fit it with a damped sine function, which gives us a periodicity of 3,91 ps, or 256 GHz. Again, this corresponds to the round trip time of an acoustic echo, as $T = 3,91ps \approx 2 \times 13.10^{-9}m \times \frac{25,7.10^{-12}s}{2\times 95.10^{-9}m} = 2d \times \frac{1}{v_{Ru}}$, where T is the periodicity, d is the film thickness and v_{Ru} is the longitudinal speed of sound in ruthenium, which we calculate with the round trip time and the film thickness of the previous experiment.

This experiment shows that it is possible to spatially restrain the depth over which an acoustic wave is generated.

V Future Steps

In order to increase the central frequency of the acoustic waves further, a first step would be down-sizing. If we assume that no other effects will arise from decreasing the layer thickness, we can calculate the layer thickness which could launch 1 THz acoustic waves in ruthenium : $d_{1THz} = \frac{v_{Ru}}{f(1THz)} = 7,39nm$, where d_{1THz} is the center wavelength of the acoustic wave, v_{Ru} is the longitudinal speed of sound in ruthenium, and $f(1THz)$ is the aimed frequency, here 1 THz.

Additionally, so as to observe time-separated high-frequency acoustic pulses, we could use bilayers. We could imagine a system of two films on top of each other, the top one being ruthenium, in which

we wish to generate the acoustic wave; and the bottom one being a material which will allow for the acoustic wave to travel through. Such architecture should circumvent the standing wave, as the acoustic wave wouldn't be bound to such a thin layer. In this geometry, we should be able to launch 1 THz acoustic waves in 7,37 nm-thick ruthenium films on top of a second material. The second material should display a similar acoustic impedance (so that the acoustic wave doesn't get reflected at the interface), and should have a low extinction coefficient and/or a low electron-phonon coupling constant and/or a high electron thermal conductivity constant (so as to launch as weak of an acoustic wave as possible in the second material). Thorough investigation has been made on the choice of material to use, which led to two candidates: gold and tungsten.

VI Conclusion

In this report, in order to increase the frequency of optically generated and detected acoustic waves in metals, we have studied the photoacoustic response of both thick, and thin films of ruthenium, and compared them with gold. We have found that ruthenium is an excellent candidate to reach such high frequencies, thanks to its remarkable electronic properties (high extinction coefficient, and high electron-phonon coupling). Furthermore, we demonstrated how restraining the layer thickness can help increase the frequency of the acoustic waves, and were able to generate 256 GHz acoustic waves in a very simple system, which goes to show how serious of a candidate ruthenium is.

Even though we were not able to reach our original aim, the research presented above in this project on the optical generation of 1 THz bandwidth acoustic wavepackets is a step forward in the direction of ultra-high frequency photoacoustic techniques for nanometer-scale alignment in tomorrow's nanophotolithography systems.

References

[1] ED. Chip machine of the future already ordered from asml in veldhoven. [En ligne le 28/07/2020] ed.nl/asml/chipmachine-van-de-toekomst-al-besteld-bij-asml-in-veldhoven~a178fbbb/.

[2] ASML. About asml : History. [En ligne le 28/07/2020] asml.com/en/company/about-asml/history/.

[3] ASML. About asml : Asml at a glance. [En ligne le 28/07/2020] asml.com/en/company/about-asml/asml-at-a-glance.

[4] ARCNL. About arcnl. [En ligne le 28/07/2020] arcnl.nl/our-mission#about.

[5] Techplayon. What is 90nm, 45nm or 5nm technology, why it ends moore's law, and what's next ? [En ligne le 28/07/2020] techplayon.com/deos-mean-90nm-45nm-5nm-technology-ends-moores-law-coming-trends-technology/.

[6] Karl Rupp. 42 years of microprocessor trend data. [En ligne le 28/07/2020] karlrupp.net/2018/02/42-years-of-microprocessor-trend-data/.

[7] Wikipedia. Moore's law. [En ligne le 28/07/2020] en.wikipedia.org/wiki/Moore\%27s_law.

[8] Tom's Hardware. Samsung plans mass production of 3nm gaafet chips in 2021. [En ligne le 28/07/2020] tomshardware.com/news/samsung-3nm-gaafet-production-2021,38426.html.

[9] Tom's Hardware. Tsmc starts $19.5 billion 3nm fab construction. [En ligne le 28/07/2020] tomshardware.com/news/tsmc-fab-3nm-5nm-process-intel-samsung.

[10] A.J. DEN BOEF. Optical wafer metrology sensors for process-robust cd and overlay control in semiconductor device manufacturing. *Surface Topography: Metrology and Properties*, 4(2):023001, 2016.

[11] S. EDWARD, H. ZHANG, I. SETIJA, V. VERRINA, A. ANTONCECCHI, S. WITTE, and P. PLANKEN. Detection of hidden gratings through multilayer nanostructures using light and sound. *Phys. Rev. Applied*, 14(1):014015, 2020.

[12] G. TAS, R. J. STONER, H. J. MARIS, G. W.RUBLOFF, G. S. OEHRLEIN, and J. M. HALBOUT. Noninvasive picosecond ultrasonic detection of ultrathin interfacial layers: Cfx at the al/si interface. *Applied Physics Letters*, 61(15):1787–1789, 1992.

[13] J.P. MONCHALIN. Laser-ultrasonics: From the laboratory to industry. *AIP Conference Proceedings*, 700(1):3–31, 2004.

[14] S. ANISIMOV, B. KAPELIOVICH, and T. PEREL'MAN. Electron emission from metal surfaces exposed to ultrashort laser pulses. *Journal of Experimental and Theoretical Physics*, 66(2):375–377, 1974.

[15] RefractiveIndex.Info. Refractive index database. [En ligne le 26/08/2020] `refractiveindex.info/`.

[16] M. BONN, D. N. DENZLER, S. FUNK, M. WOLF, S. S. WELLERSHOFF, and J. HOHLFELD. Ultrafast electron dynamics at metal surfaces: Competition between electron-phonon coupling and hot-electron transport. *Phys. Rev. B*, 61:1101–1105, 2000.

[17] D. R. LIDE. *CRC Handbook of Chemistry and Physics: SPEED OF SOUND IN VARIOUS MEDIA*. CRC Press, 1995.

[18] S. EDWARD. Detection of hidden gratings using light and sound. 2020.

[19] A. DEVOS and C. LEROUGE. Evidence of laser-wavelength effect in picosecond ultrasonics: Possible connection with interband transitions. *Phys. Rev. Lett.*, 86:2669–2672, 2001.

	Damped Sine
Equation	$\eta(t) = y_0 + A * e^{-t/t_0} * sin(2\pi \frac{t-\phi}{T})$
T	3,91 ps
R^2	0,94